Nuclear Materials and Energy 27 (2021) 100962

Contents lists available at ScienceDirect

Nuclear Materials and Energy

journal homepage: www.elsevier.com/locate/nme

TECXY simulations of Ne seeding in JET high power scenarios

P. Chmielewski [a,*], R. Zagórski [b], G. Telesca [a], M. Brix [c], A. Huber [d], I. Ivanova-Stanik [a], E. Kowalska-Strzeciwilk [a], T. Pereira [c], D.I. Réfy [e], P. Tamain [f], M. Vécsei [e], N. Vianello [g], the JET Contributors[1]

[a] Institute of Plasma Physics and Laser Microfusion, Hery Str. 23, 01-497 Warsaw, Poland
[b] National Centre for Nuclear Research, 05-400 Otwock, Swierk, Poland
[c] Culham Centre for Fusion Energy, Abingdon, UK
[d] Institut fuer Energie und Klimaforschung-Plasmaphysik Foschungszentrum Juelich GmbH, Juelich, Germany
[e] Centre for Energy Research, XII Konkoly Thege Miklós út 29-33, Budapest 1121, Hungary
[f] CEA, IRFM, F-13108 Saint-Paul-Lez-Durance, France
[g] Consorzio RFX, Padua, Italy

A B S T R A C T

Preparation of D-T experiments on JET device raises a question about the mitigation of assumed high power entering the SOL. JET DT scenarios aim to achieve good plasma confinement and the heat loads reduction to the divertor at the same time. Therefore, the divertor corner magnetic field geometry, strike point swiping and impurity seeding are considered to reduce expected high heat fluxes to the divertor plates. The aim of the paper is to analyse the influence of the neon impurity seeding on the plasma transport and its efficiency of the power mitigation in the JET tokamak as well as to perform validation of applied edge plasma model. In this contribution numerical simulations have been performed for two high power (34 MW), neon seeded DD JET discharges in the H-mode with different upstream densities and the same corner divertor configuration prepared as possible candidate for JET DT scenarios. The edge plasma transport have been described by two-dimensional multifluid TECXY code based on Braginskii plasma transport equations with assumed classical parallel transport of the plasma and anomalous perpendicular transport defined by ad hoc heat and particle transport coefficients. TECXY results show impact of the neon seeding on the reduction of the power flowing to the divertor. Scan with the neon concentration carried out for four different upstream densities allow us to determine optimal plasma conditions with the lowest target plate temperature and the lowest effective charge. Performed studies with use of the TECXY code and they comparison to experimental results give the opportunity to perform validation of applied TECXY edge plasma model and show the optimal range of plasma parameters like the upstream density and neon concentration, for which the radiation power in the SOL is the highest.

1. Introduction

Development of tokamaks and future fusion reactors with the high power flow to the Scrape-off layer (SOL) and hence to the divertor plates entails the problem of the mitigation of a large amount of energy in the SOL. The most promising candidate for the power reduction in the edge plasma is the neon impurity, which radiates mainly at SOL temperatures of about 30–50 eV around X-point [1].

Studies of the reduction of the power to the plate due to the effect of fuelling over a wide range of plasma conditions for type-I ELMy H-mode plasmas with peak radiation at the X-point reported that the minimum peak power between ELMs could not be reached [2]. On the other hand, the neon impurity seeding leads to increased divertor radiation. Additionally, the pedestal of analysed discharges with neon impurity seeding often crosses the type-I to type-III ELM regime boundary leading to compound ELMs and unsteady edge conditions [2]. However, simulations of the high power DT plasma on the basis of ELMy H-mode JPN 87412 indicate that the neon seeding controls the heat load. The neon seeding is considered to control the heat load in the high performance of the JET shots, which efficiently reduce the plate temperatures as well as keeps a good plasma performance without degradation of the fusion power [3].

It has been found that a strong neon seeding have an impact on the core, the pedestal and divertor conditions [4]. Investigations of highly radiating neon seeded H-mode plasmas in JET-ILW revealed that the plasma at both divertor target plates is in complete detachment and the pedestal density profile degradation was observed at high neon seeding. A correlation between degradation of the pedestal density, the appearance of an X-point radiation and the detachment of both targets have been found for investigated neon seeded H-mode pulses [4]. Analysis

* Corresponding author.
E-mail address: piotr.chmielewski@ifpilm.pl (P. Chmielewski).
[1] See the author list of E. Joffrin et al. 2019 Nucl. Fusion 59 11202.

https://doi.org/10.1016/j.nme.2021.100962
Received 31 July 2020; Received in revised form 10 February 2021; Accepted 3 March 2021
Available online 26 March 2021

shows that neon impurity might induce dithering between H-mode and L-mode for low heating power. It has been found that plasma can stay in H-mode for plasma heating higher than 22 MW [1].

The aim of this paper is to present the TECXY code edge plasma model and its comparison with experimental results of JET discharges prepared for DT scenarios as well as to analyse the power mitigation by neon and nickel impurities.

The paper is organized as follows. The characteristics of the JET discharges and the numerical model are described in Section 2. Simulations results and discussion are presented in Section 3, and concluded in Section 4.

2. JET discharges and the numerical model

Two high-performance H-mode JET discharges number 92432 and number 92436 have been selected for numerical analysis of the energy dissipation in the JET-DD neon seeded plasma. These discharges have been chosen for comparison of the plasmas with different values of upstream densities in a good confinement ($H_{98} \sim 1$) at high current equal to 3 MA and magnetic field equal to 2.8 T. In the JET ITER like Wall (ILW) pulse number 92432 (92436), the value of the separatrix density is about 2.0×10^{19} m^{-3} (2.2×10^{19} m^{-3}), the neon seeding via divertor valves is at the level of 6.4 el s^{-1} $\times 10^{22}$ (6.3 el s^{-1} $\times 10^{22}$) and the deuterium puff is equal to 2.1×10^{22} el s^{-1} (0.75×10^{22} el s^{-1}). Here, the neon seeding have been intended for the ion temperature measurement with the charge exchange recombination spectroscopy (CXRS) [5]. In JET pulse number (JPN) 92432, the plasma density was maintained only by gas fuelling, while the plasma density in the JPN 92436 was provided additionally by the pellet injection under low gas puff rate. Discussed pulses represent the baseline scenario pulses for

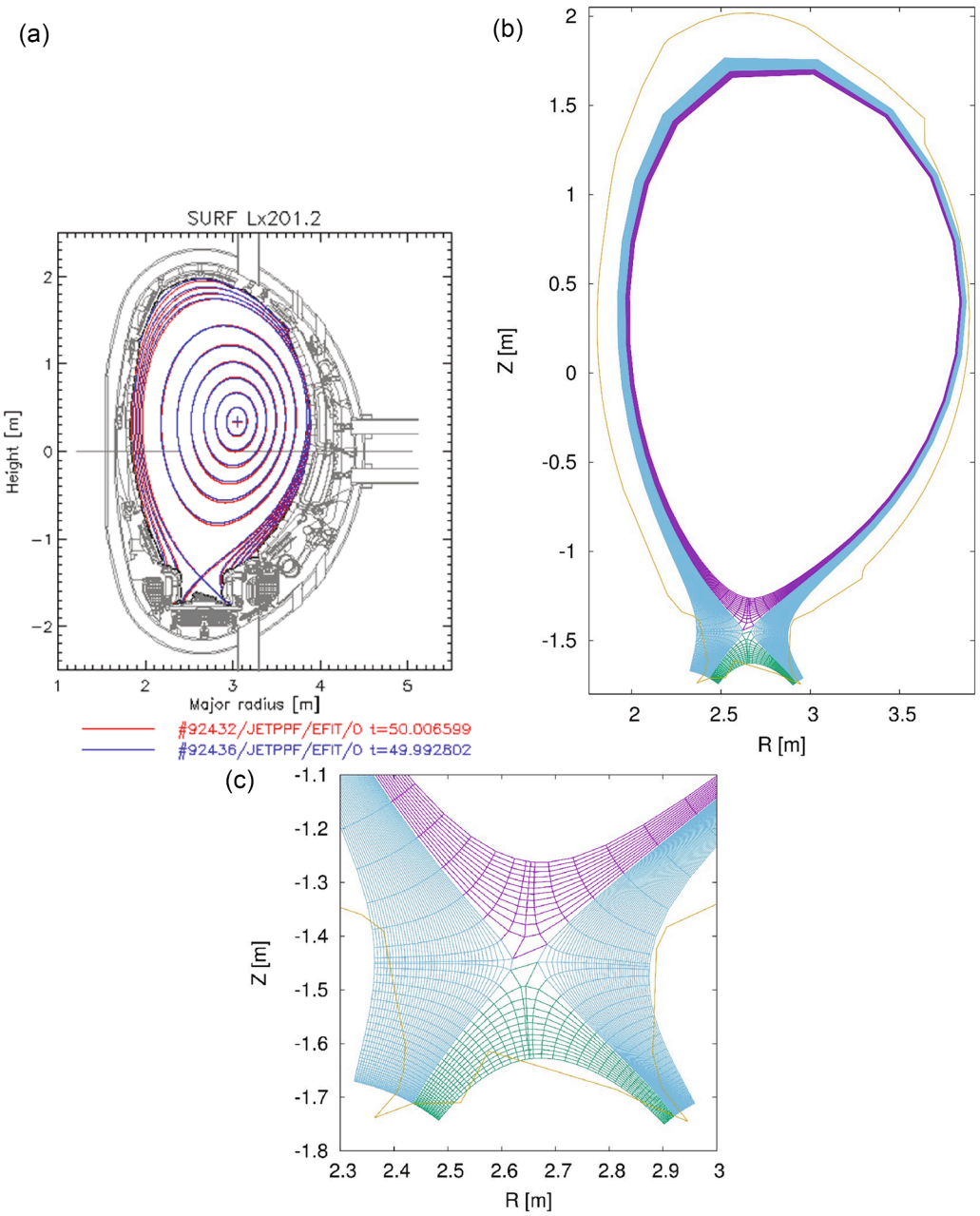

Fig. 1. The poloidal crossection of magnetic flux surfaces at $t = 50$ s (*a*) for JPN 92432 (red lines) and JPN 92436 (blue lines), the TECXY computational grid (*b*) and mesh details of the divertor region (*c*). The yellow line corresponds to the JET vessel position. (For interpretation of the references to color in this figure legend, the reader is referred to the web version of this article.)

future DT high power (~ 34 MW) discharges, which are planned in the nearest JET campaigns. Both are heated by the neutral beam injection (~ 28 MW) and the ion cyclotron resonance heating 5 MW (6 MW). A magnetic field equilibrium have been taken at $t = 50.0$ s in the JPN 92432 and identical equilibrium in the JPN 92436 at $t = 50.0$ s as well. Chosen time for the magnetic equilibrium corresponds to the phase of fully developed steady phase of the discharge with constant deuterium fuelling, constant line density and the heating (not shown). Comparison of the poloidal crossection of magnetic field surfaces is presented on Fig. 1, panel *a*. Magnetic field configuration of selected discharges corresponds to so called the corner-corner divertor configuration, where strike points are located in the divertor corner for better pumping and plasma density control [6].

The edge plasma transport model is described by set of Braginskii equations [7] with classical transport along magnetic field lines [8] and anomalous transport across field lines defined by diffusion coefficients of the order of Bohm's diffusion. Here, electrons and ions are treated as separate fluids, while plasma ions and impurity ions temperatures are assumed to be the same. Transport equations are solved numerically by the TECXY code [9–13], which involves atomic processes like ionization, recombination, excitation and charge exchange, as well as plasma-wall interaction models of chemical and physical sputtering and prompt re-deposition [14]. TECXY solves equations for few impurity species simultaneously and all ionization stages associated with these impurities. The tokamak edge plasma region is covered by the 2D, strictly orthogonal and non-uniform numerical mesh, generated on the basis of the mentioned magnetic field equilibrium (Fig. 1, *b*). The numerical mesh is shown in the *R-Z* plane of toroidal coordinates on Fig. 1, panel *b*. The mesh is denser near the divertor plates and the core region, and rare in the midplane region as well as near the tokamak wall. A typical spatial resolution of the numerical mesh close to the strike point is 1.8 mm in poloidal direction and 0.7 mm in radial direction. Here, the numerical mesh deviates significantly from the divertor plates shapes (Fig. 1, *c*) due to the strict mesh orthogonality assumption, which forces orthogonality of grid lines to magnetic field lines for each numerical cell. As a result, the actual divertor geometry cannot be considered when constructing the computational mesh. In the model, the divertor plate is perpendicular to the magnetic field line, and the strike point has the actual position on the surface of the JET tokamak plate. In **Fig. 1**c, the divertor plates considered in the model are marked with red lines, and the JET vessel is marked with a yellow line. The TECXY model of neutrals enforce a fixed shape of neutral distribution at the target plate. Therefore, the neutral model wears off potential geometrical effects, which could affect the neutral dynamic, and even large shifts of the target plate along the magnetic field lines from the original position of the plate have a negligible influence on results.

Numerical studies have been performed for JPN 92432 (JPN 92436) with the total heat power equal to 33.7 MW (34.7 MW). For numerical studies a value of the heat flux across the separatrix $P_{SOL} = 23$ MW have been assumed to be common for both JET pluses. P_{SOL} estimated as a difference of the total heat power and the plasma radiation in the core, is equal to 23.1 MW and 23.9 MW for JPN 92432 and JPN 92436, respectively. The recycling coefficients of deuterium is set constant and equal to 0.9985 at the inner and the outer target plates for main plasma, while the recycling coefficient for a high-recycling neon impurity and low-recycling nickel impurity is set to 0.925 and 0.200, respectively. As nickel is no recycling plasma impurity, the value of nickel recycling coefficient could be set zero or arbitrary low value. Here, we set the nickel recycling coefficient equal 0.2, to avoid numerical problems with value equal zero. In the TECXY model a pumping rate of the plasma is included in the recycling coefficient, which **is** defined as the total plasma flux to the divertor, Ψ_{div}, reduced by the pump-out flux and the plasma flux to the core, divided by Ψ_{div}.

The particle diffusion coefficient $D_\perp = 1$ m^{2}s^{-1} and the energy diffusion coefficient $\chi = 0.3$ m^{2}s^{-1} defines the anomalous transport of plasma across magnetic field lines. Values of $D_\perp$ and χ have been set to reproduce the experimental midplane profiles.

Neutrals are described by a semi-analytical model, in which a distribution of the neutral atom concentration is calculated on the basis of the diffusive model [15]. A value of the neutral density at the plate is calculated taking into account plasma fluxes to the target. In the case of recycled deuterium at the divertor plate two groups of neutrals are considered: fast and slow neutrals. The shape of neutral density distribution, n_N, is defined by the product of exponential functions and the neutral density at the divertor plate, n_N^{plate}, which depends on the recycling coefficient:

$$n_N = n_N^{plate} exp\left(-\frac{x_{plate} - x}{\lambda_x}\right) exp\left(-\frac{(y_{sep}(x) - y)^2}{\lambda_y^2}\right) \quad (1)$$

Here, the x (y) describes the coordinates on the numeric grid and corresponds to the poloidal (radial) direction in the tokamak geometry. For deuterium, the ionisation length $\lambda_{x,y}$ is defined for fast and slow neutrals separately and it is expressed by the ionization rate coefficient, α_i, and the rate factor for charge exchange processes, α_{cx}, as follows

$$\lambda_{x,y}^{fast} = \frac{v_{x,y}}{n_e\sqrt{\alpha_i \alpha_{cx}}} \qquad \lambda_{x,y}^{slow} = \frac{v_{x,y}}{n_e \alpha_i} \quad (2)$$

Assumed neutral distribution **has** its maximum at the strike point, $y_{sep}(x_{plate})$, and it drops exponentially along the plate to negligible values in the far SOL (second term of Eq. (1)). On the other hand, a distribution of neutrals along field lines decline exponentially with distance from the divertor plates, x_{plate}, (third term of Eq. (1)) and it is modulated by ionisation, recombination and charge exchange sources. In the case of impurities, the neutral density distribution is determined by transport processes in SOL and its shape is defined in the same way as for deuterium neutral (Eq. **(1)**). The ionization length of the pollutant atoms is defined as follows

$$\lambda_{x,y}^{Z} = \frac{v_{x,y}^{Z}}{n_e \alpha_i^Z} \quad (3)$$

where α_i^Z is the impurity atoms ionization rate coefficient.

3. Power mitigation with neon and nickel impurities

Numerical studies have been performed for the deuterium plasma with the neon and nickel impurity. Sputtering of the tungsten impurity from the divertor plates has been neglected due to the low tungsten radiation in the considered SOL region. Simulations have been performed for few chosen values of the deuterium particle flux defined at the core boundary, Γ_D, within the range of 5×10^{20} s^{-1} to 9.0×10^{20} s^{-1}. In order to find the neon impurity concentrations corresponding to the plasma radiation in the experiment, scans with different values of neon gas puff to the SOL have been done for each Γ_D value. Thereafter, based on the results of the experiments and the performed scans, a comparative analysis of the radiation of the edge plasma in the JET device and the impurity concentration will be carried out. The nickel impurity presence in the SOL plasma have been included in the additional calculations for selected cases with neon seeding.

The strike point sweeping and the divertor corner configuration applied in the considered pulses, results in the lack of the probe measurements on the outer divertor plate and missing spectral line measurements in the divertor region. Therefore, plasma conditions of the selected pulses have been reconstructed on the basis of globally calculated plasma parameters and the midplane diagnostics. On Fig. 2, there are presented radial profiles of the plasma electron density, n_e (left) and the electron temperature, T_e (right) at the outer midplane for $\Gamma_D = 7.5 \times 10^{20}$ s^{-1}. Radial distance expressed in cm is normalized to zero at separatrix. n_e and T_e radial profiles have been compared with experimental data obtained with use of the high resolution Thompson scattering (HRTS) measurements [16,17] and with additional lithium beam

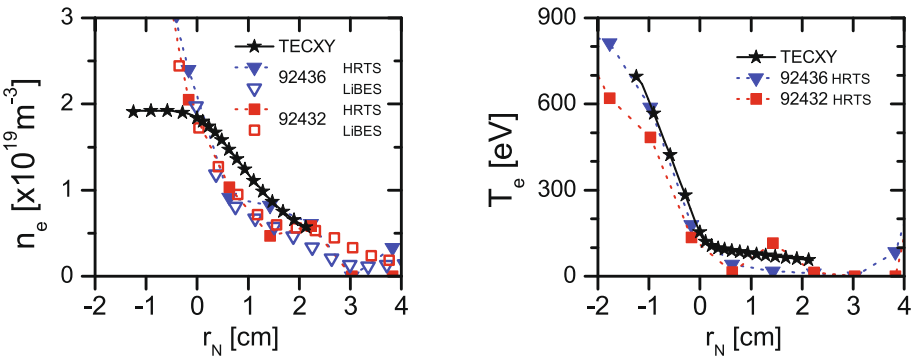

Fig. 2. Radial profiles of the electron density (left) and the electron temperature (right) at the midplane for $\Gamma_D = 7.5 \times 10^{20}$ s^{-1}. The red squares and blue reversed triangles correspond to data obtained in the JET experiment with use of Thompson scattering for JPN 92432 and JPN 92436, respectively. The empty reversed triangles and squares correspond to the density measured by the Li-BES diagnostic, while the full black stars represents data obtained in numerical simulations. (For interpretation of the references to color in this figure legend, the reader is referred to the web version of this article.)

emission spectroscopy measurements (Li-BES) for the electron density [18,19]. The density profile obtained with Li-BES have been reconstructed for the 400 ms time range (49.8 s – 50.2 s) with use of the conditional averaging technique in pre-ELM phase. The Li-BES and the HRTS diagnostics complement each other since the HRTS is a core and pedestal measurements, and loses its sensitivity outwards in the low plasma density regions, while the Li-BES is more sensitive in the SOL and loses its sensitivity invards at the high density regions. However, TECXY radial profiles of n_e and T_e are within the range of the experimental values in the SOL, whereas a discrepancy between numerical results and experimental measurements is observed in the core region for the electron density (left panel), which is a result of constant values of $D_\perp$ and χ across separatrix in the core and SOL assumed in the TECXY code. Therefore, the numerical simulations underestimate the pedestal top density, which is about 4.6×10^{19} m^{-3} for both: the HRTS and Li-BES diagnostics. Profiles of n_e and T_e slightly vary with the increase of Γ_D. The electron density at separatrix rises up to 2.2×10^{19} m^{-3} for $\Gamma_D = 9.0 \times 10^{20}$ s^{-1}, while the electron temperature drops to about 600 eV. Thereby, both profiles remain within the range of experimental measurements.

In the JPN 92432 and JPN 92436, the power to the SOL (23 MW) is reduced by the deuterium radiation as well as by the neon impurity radiation puffed from the valve localised in the divertor. On the left panel of Fig. 3, a drop of the total power to both plates have been shown vs. the neon impurity concentration, C_{Ne}, which is averaged along the separatrix. Here, the deuterium plasma radiation reduces the power to the divertor to about 20.5 MW, while puffed neon impurity enhances the power dissipation further. Mitigation of the power by neon impurity gas puff strongly depends on deuterium flux through core-SOL boundary, which is correlated with plasma density at separatrix. It has been observed that for a given neon concentration the power mitigation increases with the increase of the deuterium puff value, which corresponds to the increase of the separatrix density. On the other hand, the power mitigation improves with rise of the neon concentration for small Γ_D as well, but the value of C_{Ne} significantly exceeds experimental findings. Expected experimental power to the plate, estimated as a difference between the total input power and the total radiated power [20], is about 19 MW and have been denoted on Fig. 3 by horizontal black dashed line. This value of the power to the plate determines the neon concentration in range from 2% to 4% depending on the value of Γ_D. Value of the effective charge, Z_{eff}, averaged along the separatrix increases with the neon concentration for given Γ_D and is in the range of 3.2 and 3.6. For further analysis case of $\Gamma_D = 7.5 \times 10^{20}$ s^{-1} for $C_{Ne} =$ 3% have been selected. Notice that the highest neon impurity radiation equal to 1.6 MW (Fig. 3, right) for neon concentration about 4% has been observed for $\Gamma_D = 9.0 \times 10^{20}$ s^{-1}.

The change in the neon concentration is reflected in the plasma parameters on divertor plates. On **Fig. 4**, the total heat flux have been presented at divertor plates in the case of $\Gamma_D = 7.5 \times 10^{20}$ s^{-1}. Increase of the neon concentration results in growth of the energy dissipation and the total heat flux decrease at divertor plates. Thus, a drop of the electron temperature and growth of the electron density have been observed on both plates (**Fig. 5**). Notice, that changes of the electron density and the electron temperature values at the divertor plates corresponding to different neon concentrations are small, due to the small neon impurity radiation in the SOL. On the other hand, there is observed distorted shape of the q profile on the inner plate. Here, reduction of the heat flux near the strike point is caused by strong plasma radiation in the inner divertor region and it results in a drop of the electron temperature at strike point. The radial profiles at divertor plates reveal as well much higher heat load on the outer divertor in comparison to the inner plate.

The bolometry reconstruction of the plasma radiation for JPN 92432 and JPN 92436 is presented in Fig. 6, where a dashed violet line corresponds to separatrix position. The total power emitted by the plasma

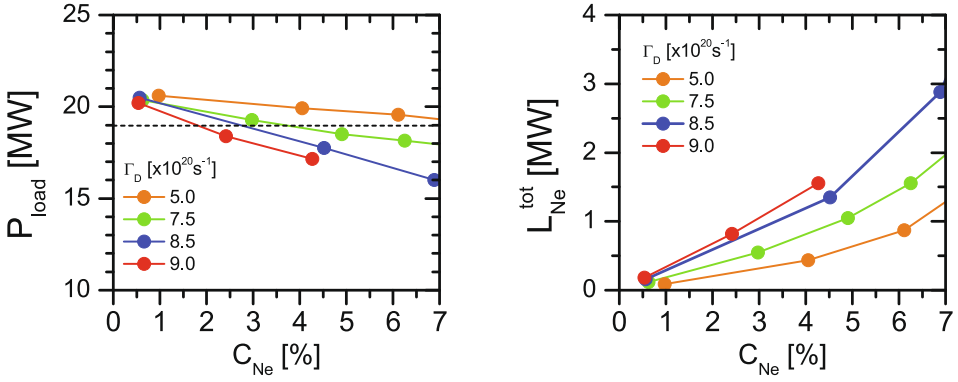

Fig. 3. Total power to divertor plates (left) and the neon line radiation (right) vs. the neon impurity concentration for various deuterium influx to the SOL. Horizontal dashed line corresponds to estimated from experimental value of the power to the plate. (For interpretation of the references to color in this figure legend, the reader is referred to the web version of this article.)

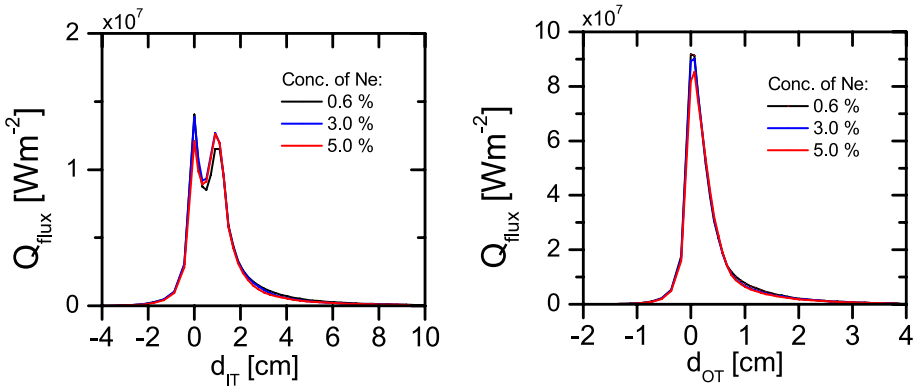

Fig. 4. Radial profiles of the total heat flux at the inner target (left) and at the outer target (right) for different neon impurity concentration under $\Gamma_D = 7.5 \times 10^{20}$ s^{-1}. Distance along the plate, *d*, have been set zero at the strike point.

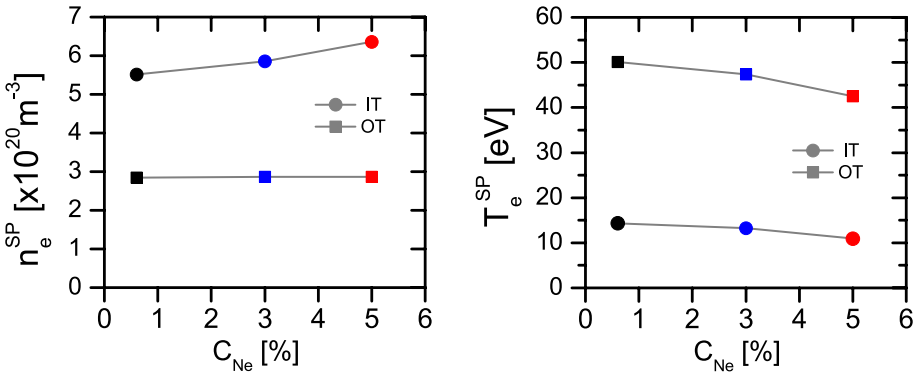

Fig. 5. Changes of the electron density (left) and the electron temperature (right) at the strike point for the inner target (circles) and the outer target (squares) vs. the neon impurity concentration under $\Gamma_D = 7.5 \times 10^{20}$ s^{-1}.

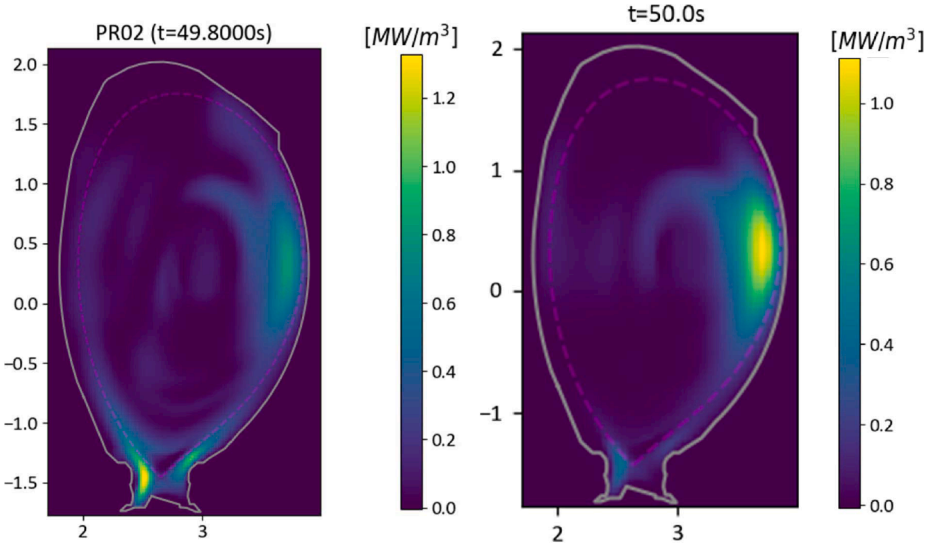

Fig. 6. Reconstruction of the radiation sources in the poloidal crossection for JPN 92432 (left) and JPN 92436 (right). Dashed violet line denotes the separatrix position. (For interpretation of the references to color in this figure legend, the reader is referred to the web version of this article.)

in the JET discharge number 92432 (92436) obtained from bolometry measurements has been calculated to be equal 13.4 MW (12.8 MW), while the plasma radiation in the SOL to be equal to 2.8 MW (2.0 MW). Most of the plasma radiation in the SOL is localised in the inner divertor and X-point region. Higher upstream electron density in JPN 92432 in comparison to the JPN 92436, results in the higher plasma radiation and a drop of the plasma temperature in the inner divertor region. Therefore, a comparison of the bolometry reconstruction for JPN 92432 and JPN 92436 reveals the impact of a growth of the separatrix electron density observed on Fig. 3. Notice that in the case of the discharge with pellet injection, the plasma radiation in the low field side of the core, is larger by 0.1 Wm^{-3} in comparison to the discharge with only neon seeding.

Analysis of distribution of the neon impurity radiation obtained in the TECXY simulations also show the neon impurity radiation concentration around X-point position, in particular in the inner divertor (Fig. 7, right). Here, the spatial profile of the Ne^{7+} line radiation in the divertor region has been obtained in the numerical simulations for $\Gamma_D = 7.5 \times 10^{20}$ s^{-1} with 3% of neon concentration. The line radiation of Ne^{7+} is the highest of all neon ionization stages and it accounts for 27% of total neon line radiation. The region of neon line radiation for lower ionisation stages is localised between X-point and divertor, while for higher ionisation stages neon radiates mostly above X-point and along the separatrix (not shown). However, other neon ionization stages radiate less energy individually in comparison to neon seven times ionized. A large part of the neon radiation, both in the experiment and in the simulations, is localised in the inner part of JET divertor as in the discussed and former JET experiments [21]. Position of the plasma radiation is directly associated with lower temperatures in the inner divertor in which plasma is semi-detached in comparison to the outer divertor and to a lesser extent in location of the neon divertor gas puffing valve.

Numerical simulations reveal also a disproportion in the power load distribution between divertor plates as the plasma first detaches at the inner divertor plate. The ratio of the power load to the inner and to the outer divertor plates is about 0.3 and slightly drops with increase of the upstream density. Such disproportion is a result of the reduction of the power flux to the inner divertor and remaining power flux to the outer plate.

Analysis of the impurity radiation in the JET plasma has been extended on the nickel impurity, which is a common element in the JET plasma. However, plasma cooling rate in the SOL at temperatures below 100 eV for nickel is equal to 10^{-30} Jm^3s^{-1} and it is two order of magnitude higher than for the neon (10^{-32} Jm^3s^{-1}) [22,23]. Concentration of the nickel in the JET discharges have been estimated on 0.5%. For this reason, there have been performed simulations with the additional nickel gas puff for constant Γ_D and neon gas puff. Numerical findings reveal that the increase of the nickel concentration even up to 1% has no significant impact on the total plasma radiation in the SOL. However, the nickel cooling rate is higher than the neon cooling rate, the nickel impurity concentration in much lower than the neon concentration, and a total nickel impurity radiation reach barely 0.2 MW in the SOL. Notice that the TECXY model of the SOL plasma does not include pedestal region, in which the nickel radiation has a significant contribution to the power mitigation.

4. Conclusions

Analysis of the impact of the neon impurity on the plasma transport and its efficiency of the divertor power mitigation in the JET tokamak have been performed. Numerical simulations based on JET-DT relevant discharges have been done with the use of the TECXY code and compared with experimental results of JET discharges prepared for DT scenarios in order to carry out a verification of the TECXY code edge plasma models. However, it has been observed that for a given neon concentration the power mitigation increases with increasing the level of the deuterium puff, the highest neon impurity radiation is equal to 1.6 MW for the neon concentration about 4% have been observed for $\Gamma_D = 9.0 \times 10^{20}$ s^{-1}. Numerical simulations show that the neon impurity radiation is not sufficient to mitigate a power in the SOL. Only with high neon seeding the radiation fraction could reach a value of 0.25, but the high neon seeding rate involves too high value of the effective charge.

Comparison of the TECXY results and experimental findings reveals few discrepancies between numerical calculations and experiment, such as low values of upstream density in simulation results for core region. Despite of mentioned discrepancies, applied model of the edge plasma allows us to describe qualitatively the plasma transport in the SOL of the JET device.

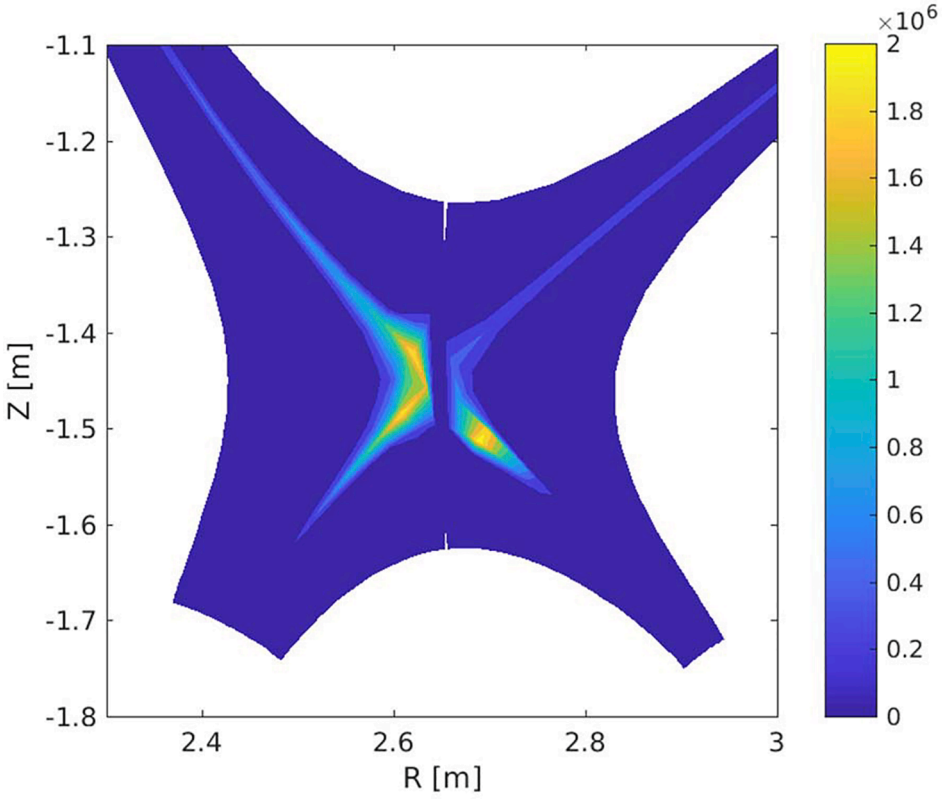

Fig. 7. Contour plot of the line radiation loses of the neon seven times ionized in the divertor region for $\Gamma_D = 7.5 \times 10^{20}$ s^{-1} with 4% of neon concentration.

CRediT authorship contribution statement

P. Chmielewski: Writing - review & editing, Writing - original draft, Visualization, Validation, Supervision, Methodology, Investigation, Formal analysis, Data curation. **R. Zagórski:** Writing - review & editing, Writing - original draft, Supervision, Software, Project administration, Methodology, Conceptualization. **G. Telesca:** Writing - review & editing, Writing - original draft, Validation, Conceptualization. **M. Brix:** Formal analysis, Data curation. **A. Huber:** Writing - review & editing, Writing - original draft, Formal analysis, Validation, Supervision, Project administration, Conceptualization. **I. Ivanova-Stanik:** Writing - review & editing, Validation, Conceptualization. **E. Kowalska-Strzeciwilk:** Writing - review & editing, Formal analysis, Data curation. **T. Pereira:** Formal analysis, Data curation. **D.I. Réfy:** Visualization, Formal analysis, Data curation. **P. Tamain:** Supervision, Project administration, Conceptualization. **M. Vécsei:** Formal analysis, Data curation. **N. Vianello:** Supervision, Project administration, Conceptualization.

Declaration of Competing Interest

The authors declare that they have no known competing financial interests or personal relationships that could have appeared to influence the work reported in this paper.

Acknowledgements

This work has been carried out within the framework of the EUROfusion Consortium and has received funding from the Euratom research and training programme 2014–2018 and 2019–2020 under grant agreement No 633053. The views and opinions expressed herein do not necessarily reflect those of the European Commission. This scientific paper has been published as part of the international project called 'PMW', co-financed by the Polish Ministry of Science and Higher Education within the framework of the scientific financial resources for 2020 under the contract No 5118/H2020/EURATOM/2020/2.

References

[1] M. Bernert, et al., Nucl. Mater. Energy 12 (2017) 111–118.
[2] C. Giroud, et al., Nucl. Fusion 52 (2012), 063022.
[3] R. Zagórski, et al., Contrib. Plasma Phys. 56 (6–8) (2016) 766–771.
[4] S. Glöggler, et al., Nucl. Fusion 59 (2019), 126031.
[5] A. Boileau, et al., Plasma Phys. Control. Fusion 31 (1989) 779.
[6] Hyun-Tae Kim, et al., Nucl. Fusion 58 (2018) 3036020.
[7] S.I. Braginskii, Rev. Plasma Phys. 1 (1965) 205.
[8] H.A. Claassen et al., Longitudinal transport coefficients of a magnetized plasma consisting of hydrogen and a single impurity element in arbitrary populated charge state, 1991. Technical Report July-2-423 Institute of Plasma Physics, Juelich.
[9] R. Zagórski, et al., J. Nucl. Mater. 266–269 (1999) 1261.
[10] H. Gerhauser, et al., Nucl. Fus. 42 (2002) 805.
[11] H. Gerhauser, et al., Nucl. Mater. 290–293 (2001) 609.
[12] R. Zagórski, et al., Contrib. Plasma Phys. 40 (2000) 405.
[13] R. Zagórski, et al., Phys. Scr. 70 (2004) 173.
[14] R. Zagórski, et al., Czech, J. Phys. 54 (2004) C15.
[15] H. Gerhauser, et al., Contrib. Plasma Phys. 40 (2000) 309–315.
[16] R. Pasqualotto, et al., Rev. Sci. Instrum. 75 (2004) 3891.
[17] J. Wesson, The Science of JET: The Achievements of the Scientists and Engineers who Worked on Joint European Torus, 2000, 1973–1999; Joint european torus.
[18] D.I. Refy, et al., Rev. Sci. Instrum. 89 (2018), 043509.
[19] M. Brix, et al., Rev. Sci. Instrum. 83 (2012) 10D533.
[20] G. Telesca, et al., Nucl. Fusion 59 (2019), 056026.
[21] B. Lomanowski, et al., Nucl. Mater. Energy 20 (2019), 100676.
[22] A. Kallenbach, et al., Plasma Phys. Control. Fusion 55 (2013), 124041.
[23] D.E. Post, et al., At. Data Nucl. Data Tables 20 (5) (1977) 397–439.